CATAL. REV.—SCI. ENG., 42(4), 481–510 (2000)

Carbon Nanofibers: Catalytic Synthesis and Applications

KRIJN P. DE JONG* and JOHN W. GEUS

Inorganic Chemistry and Catalysis
Utrecht University
P.O. Box 80083
3508 TB Utrecht, The Netherlands

Key Words: Carbon; Graphite; Carbon nanofibers; Carbon nanotubes; Carbon filaments; Filamentous carbon; Catalytic synthesis; Catalyst support; Gas storage.

*To whom correspondence should be sent.

ABSTRACT

Carbon nanofibers (diameter range, 3–100 nm; length range, 0.1–1000 μm) have been known for a long time as a nuisance that often emerges during catalytic conversion of carbon-containing gases. The recent outburst of interest in these graphitic materials originates from their potential for unique applications as well as their chemical similarity to fullerenes and carbon nanotubes. In this review, we focus on the growth of nanofibers using metallic particles as a catalyst to precipitate the graphitic carbon. First, we summarize some of the earlier literature that has contributed greatly to understand the nucleation and growth of carbon nanofibers and nanotubes. Thereafter, we describe in detail recent progress to control the fiber surface structure, texture, and growth into mechanically strong agglomerates. It is argued that carbon nanofibers are unique high-surface-area materials (~200 m^2/g) that can expose exclusively either basal graphite planes or edge planes. Subsequently, we will present the recently explored applications of carbon nanofibers: polymer additives, gas storage materials, and catalyst supports. The latter application is described in detail. It is shown that the graphite surface structure and the lyophilicity play a crucial role during metal emplacement and catalytic use in liquid-phase catalysis. A case in point is fiber-supported Pd catalysts for nitrobenzene hydrogenation. Finally, we summarize issues with respect to the large-scale production of carbon nanofibers, including production cost estimates and research items to be dealt with in future work.

I. INTRODUCTION

The history of carbon nanofibers goes back more than a century. In a patent published in 1889 [1], it is reported that carbon filaments are grown from carbon-containing gases using a metallic crucible as—probably unintentional—the catalyst. Robertson [2] was among the first to recognize that the interaction of methane and metal surfaces led to graphitic carbon at relatively low temperatures. For the first 80 years of this century, the occurrence of carbon nanofibers—then often referred to as carbon filaments or filamentous carbon—was considered a nuisance. The fibers often occurred in metallic catalysts used for the conversion of carbon-containing gases (e.g., in Fischer–Tropsch or steam–methane reforming reactions). A typical example of a transmission electron micrograph (TEM) of a thus affected catalyst is shown in Fig. 1. Next to destruction of the catalyst structure on a microscopic scale, complete destruction of catalyst pellets [3], attack of reactor walls, and rupture of reactor walls have been observed in industrial practice. In order to suppress the formation of these harmful fibers, detailed mechanistic studies were carried out on their nucleation and growth. These studies have been proven extremely useful and they are concisely described in Sect. II of this review.

In the 1980s, several workers have explored the use of carbon nanofibers for such applications as additive in polymers and as catalyst support material.

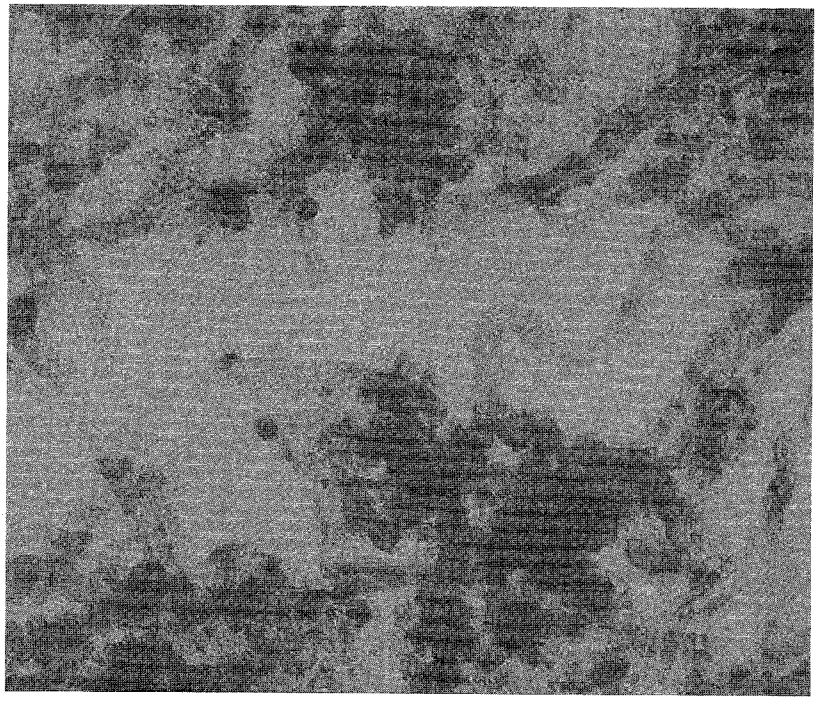

FIG. 1. Transmission electron micrograph of carbon nanofibers formed from methane decomposition at 843 K on an Ni/γ-Al_2O_3 catalyst.

There was a desire to control the properties of the fibers: surface structure (basal versus edge planes of graphite), diameter and length of the fibers, texture, mechanical strength, and the extent of agglomeration of the fibers to make strong, macroscopic bodies. This work is presented in detail in Sect. III.

An article by Iijima [4] that showed that carbon nanotubes are formed during arc-discharge synthesis of C_{60}, and other fullerenes also triggered an outburst of the interest in carbon nanofibers and nanotubes. These nanotubes may be even single walled, whereas low-temperature, catalytically grown tubes are multiwalled. It has been realized that the fullerene-type materials and the carbon nanofibers known from catalysis are relatives and this broadens the scope of knowledge and of applications. An excellent description of these developments can be found in the book edited by Ebbesen [5]. It has been realized, however, that arc-discharge and laser-ablation methods lead to mixtures of carbon materials and thus to a cumbersome purification to obtain nanofibers or nanotubes [6]. From an application point of view, we think that catalytic growth of nanofibers as described in this review is most promising.

Applications of carbon nanofibers that are dealt with in Sect. IV of this review are polymer additives, gas storage, and catalyst support materials. The first application has already turned into a commercial exploitation of these materials. Gas storage applications are very much in an exploratory stage, although these

attract much attention due to reports on spectacular hydrogen uptake capacities. The application dealt with here in detail is that of catalyst support material. Metals emplacement studies as well as the usage of Pd/C–nanofiber catalysts for nitrobenzene hydrogenation are based on recent work in our laboratory.

In Sect. V, we will describe the issues around large-scale production of carbon nanofibers. The overall economics are affected by the fiber yield, the feedstock used, the rate of growth, and the reactor technology. Overall production-cost estimates of carbon nanofibers are presented. In Sect. VI, we discuss the outlook of the use of carbon nanofibers as well as future research needed. A summary and conclusions can be found in Sect. VII.

II. CATALYTIC GROWTH

In this section, we review some of the literature mainly from the period 1980–1997 that involves the basic phenomena of growth. Some of this and earlier literature has been described more extensively in reviews by Trimm [7], Rostrup-Nielsen [8], Bartholomew [9], Figueiredo [10], Baker [11], and Rodriguez [12]. Here, we focus on the overall picture, the thermodynamics, the nucleation, and growth, followed by a mechanistic picture. Finally, some comments are made on how to prevent the growth of fibers, which is still relevant to those who consider carbon nanofibers as their enemies rather than as their friends.

The most important metals to catalyze the growth of graphitic carbon nanofibers are (alloys of) iron, cobalt, and nickel; chromium, vanadium, and molybdenum have also been studied [12]. The metals have been used both as bulk particles (size typically 100 nm) and as supported particles (10–50 nm). Importantly, all of these metals can dissolve carbon and/or form metal carbides. Typically, methane, carbon monoxide, synthesis gas (H_2/CO), ethyne, and ethene in the temperature range 700–1200 K are employed to provide carbon atoms.

The general schematic picture that has emerged for nanofiber formation is shown in Fig. 2. The hydrocarbon molecules decompose on the free-metal surface and form carbon atoms with concomitant desorption of molecular hydrogen. The carbon dissolves in and diffuses through the bulk of the metal—although some contribution of surface diffusion cannot be excluded—and precipitates in the form of graphite at the other side of the metal particle. This mechanism has been proposed and confirmed many times [8,10,13–18].

First, it is important to understand the thermodynamics of the process. It has been recognized for over 50 years that the driving force needed to precipitate the graphitic carbon fiber is larger than that expected on the basis of the thermodynamic stability of bulk graphite [19]. In Fig. 3, data from De Bokx et al. [15] show the equilibrium gas composition during the (steady state!) decomposition of methane to hydrogen and graphitic nanofibers. Clearly, the methane gas pressure needed to grow the fibers is larger than that needed to form bulk graphite (solid line). In the 1980s, an intense debate continued on the implication of the

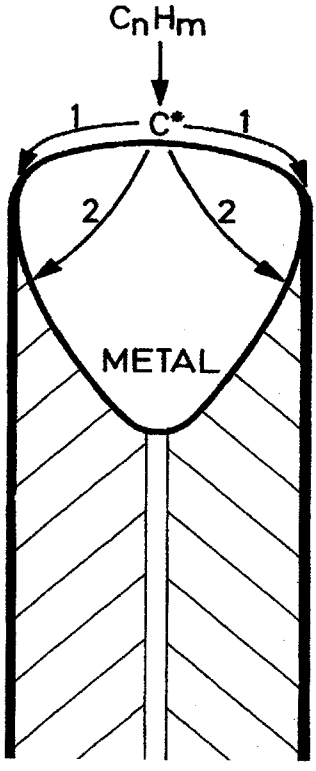

FIG. 2. Schematic picture of the metal-catalyzed growth of a carbon nanofiber from gaseous hydrocarbons. (Reproduced with permission from Ref. 10.)

apparent lower thermodynamic stability of the fibers vis à vis graphite. It has been suggested that the (enhanced) surface energy of the fibers contributed to their lower thermodynamic stability [20], an argument later on denied by, for example, De Bokx et al. [15]. The latter authors suggested that intermediate metal carbide has to be formed that decomposes into graphite and the metal. In Fig. 3, we have added data based on the stability of stoichiometric nickel carbide, Ni_3C, that show that this compound can be formed during steady-state growth of the fibers, in particular at lower temperatures. Additional evidence from magnetic measurements (*vide infra*), however, makes the presence of Ni_3C unlikely under steady-state growth conditions. Later, Alstrup [18] formulated the growth process as formation of subsurface carbide that forms the source for carbon atoms to diffuse through the bulk of the metal particle (Fig. 2). In other words, the driving force for growth is a concentration gradient of carbon atoms from the metal–gas surface to the metal–graphite surface [16,21].

Although the above rationalizes the steady-state growth, it does not touch upon the important question of the nucleation phase. Clearly, under many conditions, graphitic carbon fibers do not grow, although the gas-phase composition

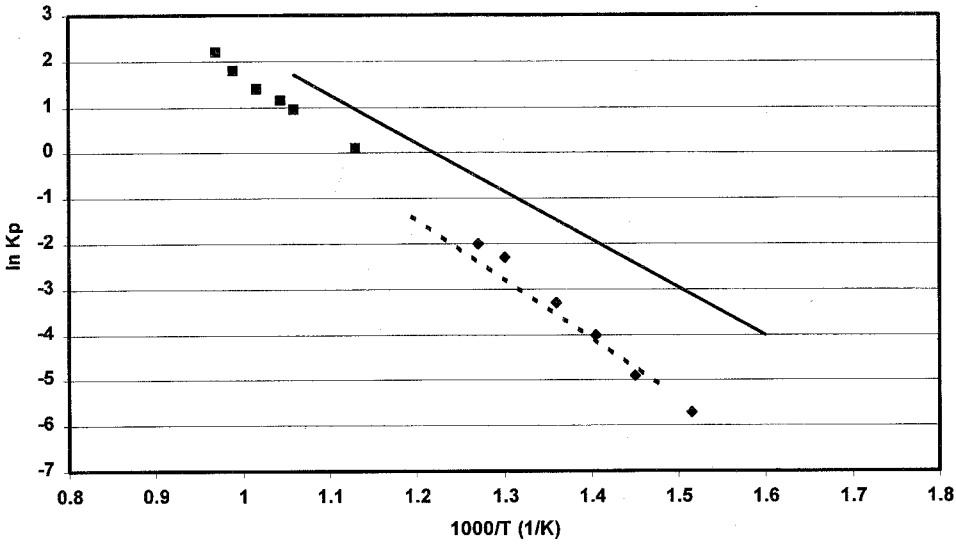

FIG. 3. Gas-phase compositions (hydrogen/methane) in equilibrium with graphite (solid line), growing carbon fibers (experimental points for Fe and Ni), and Ni_3C (broken line) as a function of temperature. ◆: Nickel; ■: iron; solid line: graphite; broken line: nickel carbide. (Data from Refs. 15 and 16.)

allows for fiber growth according to the data shown in Fig. 3. The nucleation phase of the carbon fibers has been studied in detail by Kock et al. [16] and by Hoogenraad [22], using magnetic measurements. Here, we summarize the latter study using a nickel-based catalyst and methane to grow the fibers.

In Fig. 4, the amount of carbon with respect to nickel, present on an alumina support, has been plotted versus time (Fig. 4A). The carbon in this experiment

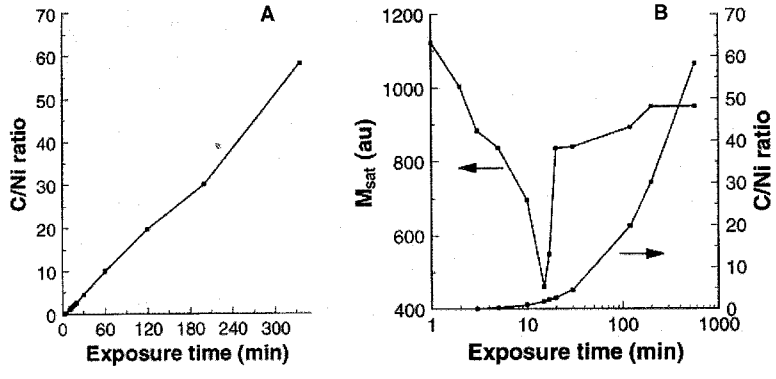

FIG. 4. Nucleation and growth of carbon fibers on a nickel-on-alumina catalyst. (A) C/Ni atomic ratio with time on a linear scale. (B) Saturation magnetization and C/Ni ratio with time on a logarithmic scale. (Reproduced from Ref. 22.)

was deposited from methane at 843 K, whereas the C/Ni atomic ratio was calculated from gas-phase analysis data. The almost linear increase of the C/Ni atomic ratio with time may suggest a smooth nucleation process. As we will discuss, this is not the case and it points to the limited value of gravimetric studies on carbon deposition to unravel the details of the fiber-growth process.

In the study by Hoogenraad [22], the sample of Ni/γ-Al_2O_3 exposed to methane at 843 K has been cooled down and the saturation magnetization (M_{sat}) of the system has been measured using a vibrating-sample magnetometer. Much care has been taken to check that the system did not change during cooling down and sample transfer. The results obtained are shown in Fig. 4B on a logarithmic scale for reasons of clarity only. During the first 12 min of exposure to methane, a strong drop of M_{sat} occurs with a sudden increase thereafter. Again, the C/Ni smoothly increases during the entire period. The most likely explanation for this reads that the formation of nonferromagnetic nickel carbide occurs in the first phase of the growth process. We think that at that time no fibers are present as yet. Suddenly, after 12 min, the magnetization restores due to decomposition of nickel carbide into ferromagnetic nickel and graphite. Steady-state growth then occurs on metallic nickel with some dissolved carbon to assure transport to the metal–graphite interface.

On the basis of these very important results, Hoogenraad [22] has proposed the model for nucleation and growth shown in Fig. 5. Methane decomposes into carbon and hydrogen atoms at the nickel surface (2). H_2 molecules desorb and carbon dissolves and forms a (substoichiometric) nickel carbide (3). This nickel carbide is metastable with respect to nickel metal and graphite. After, say, 10 min, the carbide phase decomposes into metallic nickel and graphite that encapsulates the nickel particle in question (4). According to Hoogenraad, the metal particle is squeezed out because of pressure buildup due to the formation of graphite layers at the internal surface of the graphite envelope, on the one hand, and liquidlike behavior of the metal under these conditions, on the other (5). As soon as the metal is pushed out, the fresh surface is exposed to the methane and growth continues. Finally, a steady-state process occurs with either pulsed growth (6a) or smooth growth of a straight fiber (6b). This model also explains why, more often than not, metal particles are found at the tip of the carbon fiber: The graphite fiber pushes the metal particle from the support and continues to grow at "the back of the particle."

From the model presented, the precipitation of graphite from metastable nickel carbide is crucial for the start of fiber growth. Another effect of graphite precipitation though may be disintegration of metal particles, as has been noted by Lee and Ruckenstein [23].

In addition to the model presented in Fig. 5, it has been stressed by a number of workers [18,24] that the detailed surface structure of the metal may play a role in the growth process. Alstrup [18] related the fact that the Ni(110) and Ni(100) surfaces are much more active for methane dissociation than is the Ni(111) surface [25,26] to the growth of carbon fibers. It has been concluded that during growth,

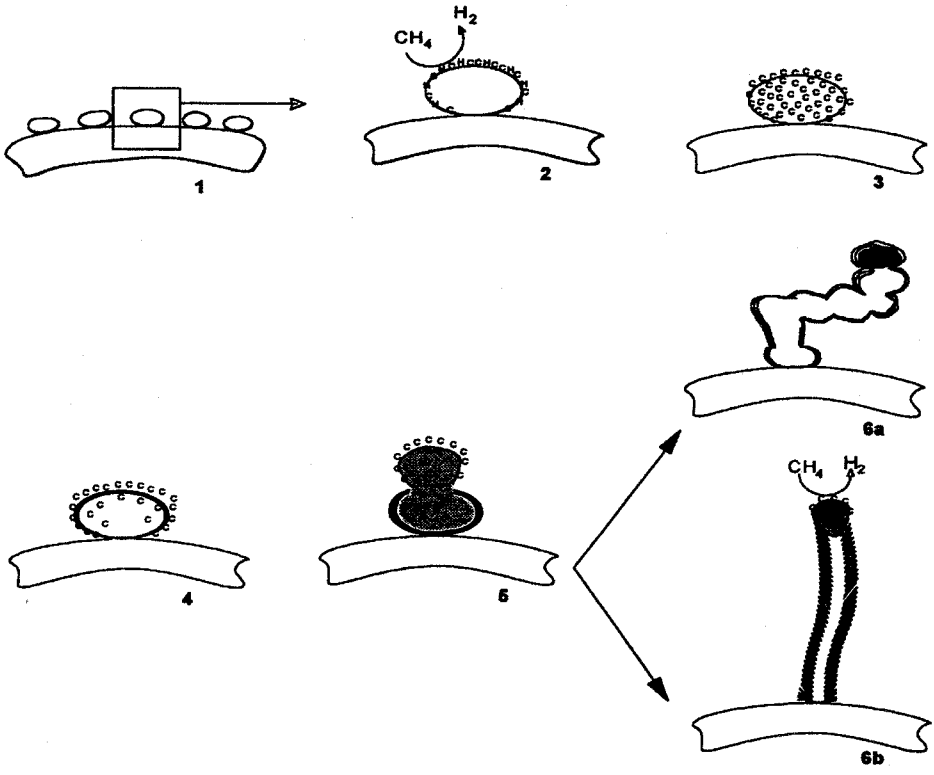

FIG. 5. Mechanism for the nucleation and growth of a carbon nanofiber from methane catalyzed by a supported metal particle. (Based on the work of Hoogenraad [22].)

a nickel particle exposes the more open surfaces to the gas phase, and the (111) planes epitaxially grow graphite.

The above comments on faceting of the metal particles are in line with electron microscopy observations. Audier et al. [24] have performed elegant electron microscopy using metal-alloy particles showing the anisotropy of the fiber growth. In Fig. 6, faceted nickel particles on top of carbon fibers are shown that have been reproduced from the work of Zaikovskii [27]. Faceting of the metal particle to allow for both hydrocarbon dissociation and graphite precipitation constitutes a reasonable alternative for the nucleation phase described in Fig. 5 (part 5). Electron-diffraction experiments by Yang and Chen [28] provide further details on the structure of the nickel planes in contact with the gas phase and graphite fiber, respectively (Fig. 7). It should be noted, however, that all of these observations on metal-particle faceting inevitably had to be carried out after cooling down the sample; this can invoke crystal shape changes.

For unsupported metal particles, the model shown in Fig. 8 and proposed by Baker et al. [29] explains that more than one fiber can grow from a metal particle. The faceting of the metal particles is such that hydrocarbons dissociate

FIG. 6. Faceted crystalline nickel particles at the top of carbon nanofibers. (Reproduced with permission from Ref. 27.)

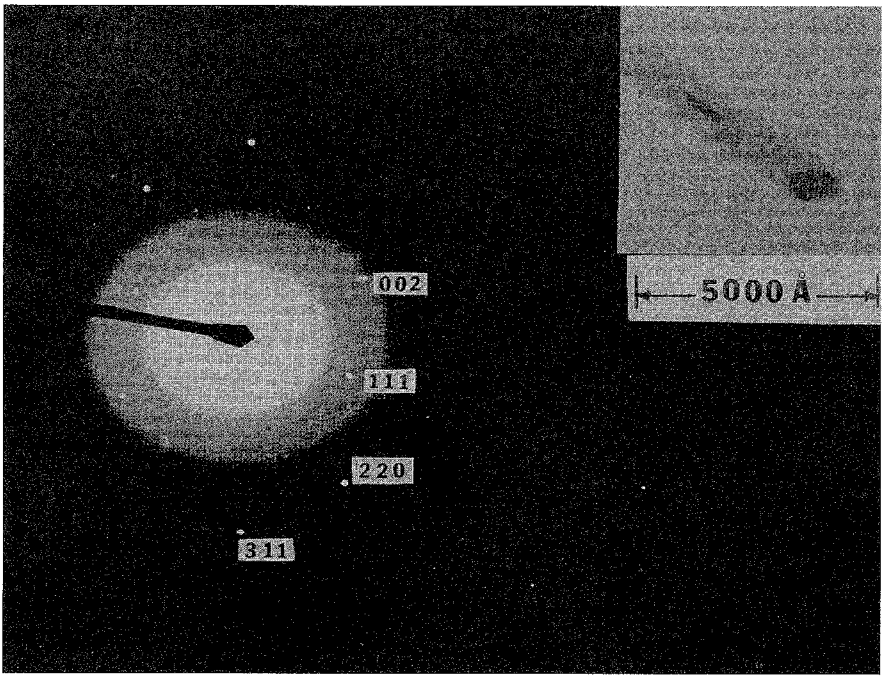

FIG. 7. Electron-diffraction pattern of a nickel particle present at the end of a carbon fiber. (Reproduced with permission from Ref. 28.)

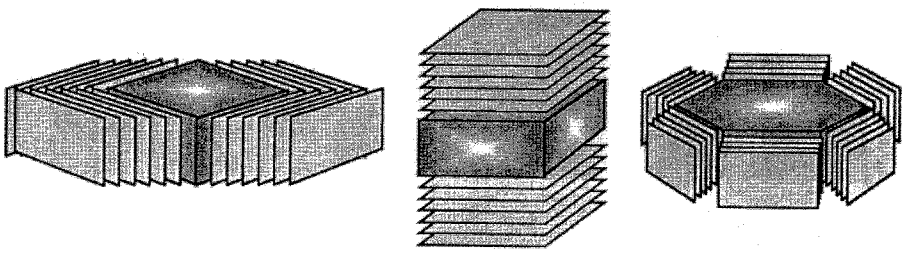

FIG. 8. Schematic picture of unsupported faceted metal particles that allow growth of multiple fibers with "herringbone" or "deck of cards" morphology. (Reproduced with permission from Ref. 29.)

at the free planes and carbon atoms migrate through the bulk of the metal and precipitate at other faces. In our opinion, Fig. 8 suggests a faceted shape of the fibers too; this has never been observed with electron microscopy, though.

The models developed for carbon fiber growth are applied to develop rational designs for the synthesis of carbon fibers with desired properties. Here, we note that much of the work cited originally has been done to develop tools to suppress carbon formation in metal catalysts. We will not discuss the latter subject in any detail. Here, it suffices that the models sketched in Figs. 5 and 8 have proven very useful in that respect. The first and simplest measure is to add (relatively large amounts of) sulfur to poison the hydrocarbon dissociation [3]. Alloying the active metal (say Ni) with an inactive metal (say Cu) may reduce the solubility of carbon sufficiently to suppress growth, although other special (octopus) types of fiber may develop [17]. Very small particles also appear to inhibit graphite nucleation. Enhanced metal–support interaction may prevent the particle from being lifted from the surface, again preventing graphite nucleation. In line with this, Lee and Ruckenstein [23] have suggested that carbon filaments appear only under conditions that the interfacial free energy between metal and substrate is larger than the sum of those between carbon and substrate, and carbon and metal. Finally, doping of metals with oxides has been proven useful to suppress carbon fiber growth.

III. PROPERTIES

A. Primary Structure: Surface Structure, Fibers, Tubes

It has turned out that the surface structure of carbon fibers can be controlled. In Fig. 9A, a high-resolution TEM picture of a nanofiber that exposes only basal planes of graphite is shown. From the phase contrast, individual graphite layers are visible. This type of carbon fiber can be grown from iron [28,30–32] and cobalt [33–36] particles as well as from nickel particles at elevated temperatures [21,37,38]. In Fig. 9B, we show a fiber with only graphite edge sites being ex-

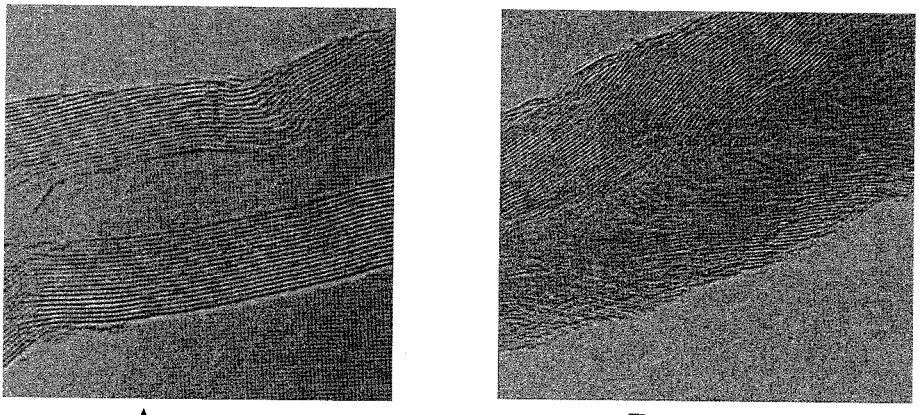

FIG. 9. High-resolution TEM micrographs from parallel (A) and fishbone (B) carbon nanofibers.

posed; this is often referred to as fishbone-type fibers by Geus and co-workers [22,39,40] or as herringbone fibers by Baker and co-workers [29]. The fishbone-type fibers have been mainly observed with nickel and nickel–iron alloy and methane as the carbon source. We know no systematic study of the relationship between the nature of the carbon-containing gas and the structure of the resulting carbon nanofibers.

Figure 10 shows simplified models for the structure of parallel and fishbone-type fibers. The growth of parallel fibers using iron as the catalyst has been studied in detail by high-resolution transmission electron microscopy (HR-TEM); see Fig. 11 [27]. It is noted that the graphite layers grow at an angle with the iron surface, thus leading to parallel fibers. The faceting of nickel particle in combination with epitaxy of graphite and Ni(111) rationalizes fishbone-type fibers (cf. Fig. 8, left). Apparently, with iron, the strong interaction between graphite and metal is less structure sensitive than with nickel. This may be related to higher carbon concentrations in iron than in nickel during steady-state growth.

The parallel fibers always display a hollow core, as apparent from Fig. 9A. In that respect, these are often referred to as carbon nanotubes, strongly related to those produced by arc-discharge methods [4]. Snoeck et al. [21] have provided an elegant model explaining why full or hollow fibers are formed from supported metal particles. Briefly, at low temperature, nucleation is slow and carbon atoms have reached the entire metal–support interface via diffusion and nucleation of a full fiber is apparent. At more elevated temperatures, the nucleation starts before the entire metal–support interface has been saturated with carbon atoms; for geometric reasons, the nucleation starts at the interface among the metal/support/gas phase, which leads to hollow fibers. Intermediate forms have also been observed [41]. The mechanism is further illustrated in Fig. 12. Extreme temperatures (>1300 K) may now be expected to lead to single-walled carbon nanotubes (SWNT) also from

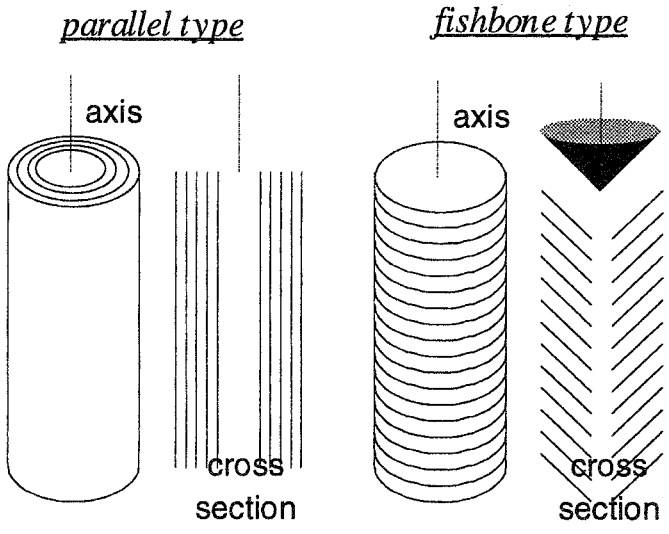

FIG. 10. Simplified representation of the structure of parallel (left) and fishbone type (right) carbon nanofibers. The cross sections shown relate to the projections as observed with TEM. (Reproduced from Ref. 22.)

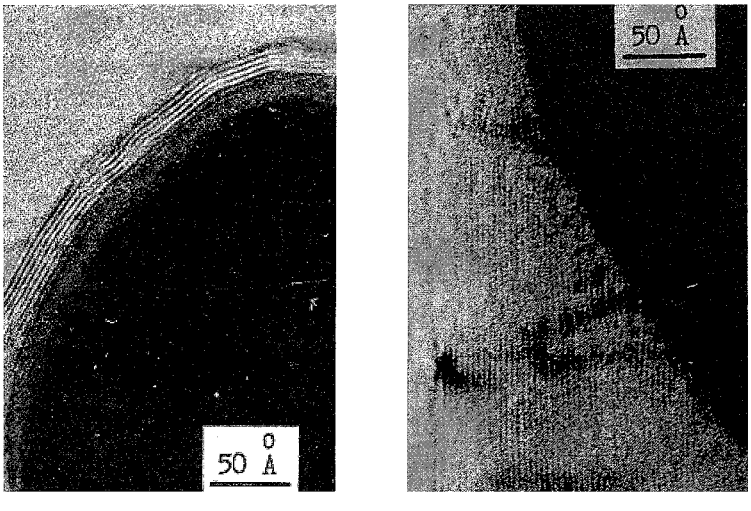

FIG. 11. Graphite structures at the iron particle. Left: Upper part with graphite planes parallel to the iron surface. Right: Lower part in contact with the carbon fiber; here, the graphite planes have grown at an angle with the iron surface, giving rise to a parallel fiber structure. (Reproduced with permission from Ref. 27.)

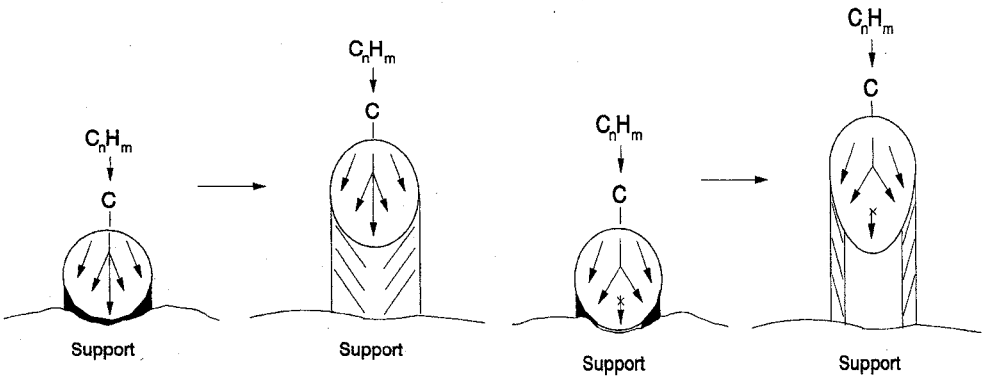

FIG. 12. Schematic picture of the formation of a full fiber (left) and a hollow tube (right). In the case of the fiber, the nucleation has taken place over the entire back of the metal particle; in the case of the tube, the nucleation has been restricted to the vicinity of the gas–metal interface. (Reproduced with permission from Ref. 21.)

catalytic growth, a phenomenon that has been reported recently by Colomer and co-workers [42]. Interestingly, Kitiyanan et al. [43] have obtained SWNT with high selectivity at more moderate temperatures (973 K) using a CoMo-based catalyst.

Having discussed the surface structure, we mention that the graphite structure present in these fibers is turbostratic graphite. This is apparent from the *d*-spacing along the *c* axis: ~0.340 nm for these fibers and 0.334 nm for well-crystallized graphite. Apparently, within the growth process, ordering of atoms within a graphene layer is high, but between layers, it is limited. On the one hand, this reflects the much stronger bonding within a layer. However, it may also provide insight in the detailed mechanism of layer formation and stacking.

In conclusion of this section, we mention that the surface structure of carbon nanofibers may be varied between extremes (i.e., graphite basal versus edge planes). It is probably the only carbon material known to date that combines high surface area with this high specificity of a certain type of surface site. We mention, however, that the conclusion on the surface structure has been based on indirect evidence by TEM and that, as yet, hardly any direct information on the detailed nature of surface sites has been gathered. One may wonder, for example, how the graphene layers terminate in fishbone fibers.

B. Secondary Structure: Diameter, Length, Shape, Texture

Whereas the primary structural features discussed in Sect. III.A have been studied in detail, the secondary features mentioned here have received less attention. The diameter of the fibers can be varied by variation of the metal particle size. For a single fiber—so much studied by TEM—this is not problematic. If we want to vary the fiber diameter for a macroscopic sample, however, we need

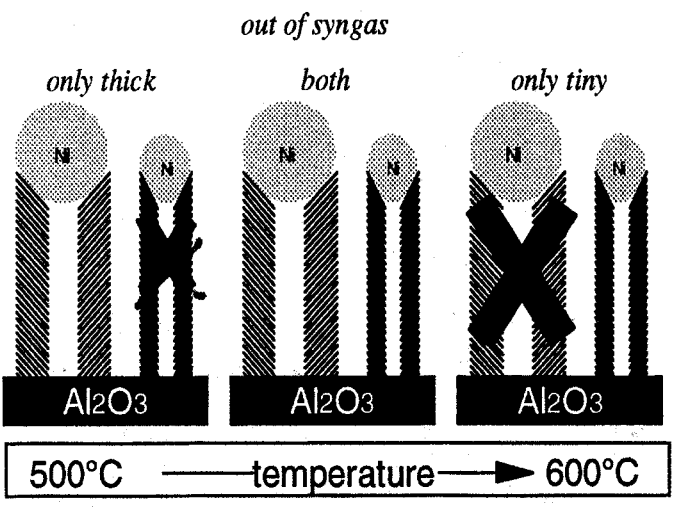

FIG. 13. Schematic presentation of the growth of carbon fibers at different temperatures from synthesis gas over a Ni-based catalyst. (From Ref. 22.)

a narrow metal particle size distribution. The latter demand calls strongly on the synthesis of the metal precursor. Hoogenraad [22] has taken an alternative approach. By selection of the growth conditions, he was able to selectively grow either thin, thick, or both thin and thick fibers from a single metal catalyst (Fig. 13). Using CO/H_2 as the carbon source, by variation of the temperature only thick (~35 nm), both thick and thin, and only thin (~12 nm) fibers were obtained.

From the revealing *in situ* electron microscopy work of Baker et al. [13], we know that the rate of fiber growth (in nm/s) increases with decreasing metal particle size (Fig. 14). In other words, thin fibers grow more rapidly than thick fibers. Furthermore, growth is regularly interrupted by encapsulation of the metal particle, followed by growth in a different direction. These two facts together cause thin fibers to display a straight shape over longer distances than thick fibers. This conclusion has impact on the tertiary structure of the fibers and their related mechanical strength (Sect. III.C).

The length of fibers is difficult to study. In general, one can say that the aspect ratio of fibers is huge and that the length of fibers can be as high as 1 mm or even beyond. Most recently, Abatemarco et al. [44] have tried with some success to control the length (1–3 μm) by fractionation of as-synthesized material using microfiltration. Jia and co-workers [45] have reduced the micrometer length to the nanometer length by ball milling and by boiling in concentrated nitric acid. The latter method gave rise to a fiber length inversely proportional to boiling time.

Next to length, the mesoscopic shape of the fibers is relevant. We have already referred to the relation between straight fiber and fiber diameter, but also other shape phenomena are apparent. In her review, Rodriguez [12] mentions in

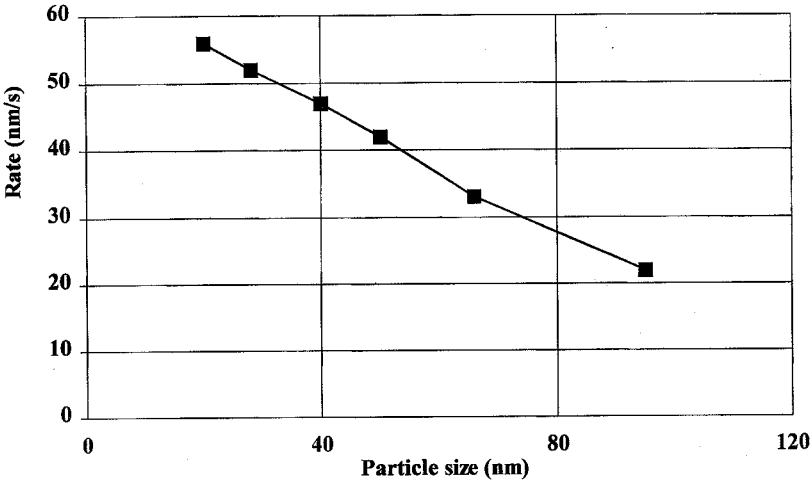

FIG. 14. The variation of the linear growth rate of carbon nanofibers from ethyne at 1010 K with the iron–metal particle diameter. (Data from Ref. 13.)

addition to straight fibers, bi-directional, twisted, helical, and branched fibers. For a detailed discussion on the relation between metal and different shapes, we refer to Ref. 12. For the helical fibers to form, several models have been proposed. Rodriguez mentioned an occasional rotary motion of metal particles, whereas Rostrup-Nielsen and Trimm [8] ascribed this to screw dislocations in the metal particle surface. Amelinckx and co-workers [46] described the process of spiral growth more quantitatively by invoking the concept of a spatial hodograph related to anisotropic growth rates that leads to a rotating growth front. It is noted that the spirally wound fibers have been grown by the latter workers using cobalt particles and ethyne at 873–973 K. Studying the nickel-catalyzed growth of carbon microcoils (fiber diameter, 1–2 μm), Motojima and co-workers [47,48] proposed the anisotropy of the carbon deposition rate on different nickel crystal planes to cause the spiral growth.

The fiber secondary structure gives rise to the textural properties—in particular, surface area and pore volume. In Table 1, we have gathered some data on the texture as reported in the literature. In general, one can say that the fibers do not contain micropores and that the surface area can range from 10 to 200 m^2/g and the mesopore volume ranges between 0.50 and 2.0 mL/g. Note that these pore-volume data are obtained with fibers as-grown. Specific treatments in the liquid phase can be applied to largely reduce the pore volume and to obtain much denser and compact fiber structures [53].

C. *Tertiary Structure and Mechanical Properties*

Compared to the large volume of literature on the mechanism of growth, the studies on the macroscopic, mechanical properties of bodies consisting of ag-

TABLE 1

Texture of Carbon Nanofibers from Different Literature Sources

Catalyst	Growth	CNF surface area (m^2/g)	CNF pore volume (mL/g)	Ref.
$Ni/\gamma\text{-}Al_2O_3$	Methane, 843 K	65	0.50	49
$Ni/\gamma\text{-}Al_2O_3$	Syngas, 803 K	95	0.95	49
$Ni/\gamma\text{-}Al_2O_3$	Syngas, 843 K	120	0.70	49
$Fe/\gamma\text{-}Al_2O_3$	Syngas, 843 K	230	1.60	50
Fe bulk	Syngas, 873 K	184	n.a.	51
Fe/CNF (?)	"Hyperion"	178	n.a.	52

glomerates of carbon nanofibers have been limited in number. The work of Hoogenraad in our laboratory [22] is one of the few studies providing some clues, whereas the recent paper of Kushvinov et al. [54] gives a comprehensive phenomenological description. Moy and Chishti [55] give a useful description of the tertiary structures that can be obtained; that is, "bird nests," "open net," and "combed yarn."

In general, porous bodies of carbon nanofibers are grown from porous supported metal catalyst bodies in the size range of micrometer to millimeter. Under many growth conditions, a single body of, say, Ni/Al_2O_3 grows out to a single body of porous carbon, inevitably of a larger size. Depending on the growth conditions, Hoogenraad [22] observed that unloading of the reactor led to powdery material (formed from body disintegration) via larger but weak bodies to large, mechanically strong conglomerates (Fig. 15). In this work, the large differences between the growth conditions are related to the Ni-crystallite size responsible for growing the carbon fibers (cf. Fig. 13). When rapidly grown, thin (~12 nm) fibers are predominantly present in the carbon structure; their straightness will lead to limited interweaving and thereby bodies of limited strength (Fig. 15A). When slowly grown, thick (~35 nm) fibers predominate, interweaving is pronounced and thereby the mechanical strength of the bodies is high (Fig. 15C).

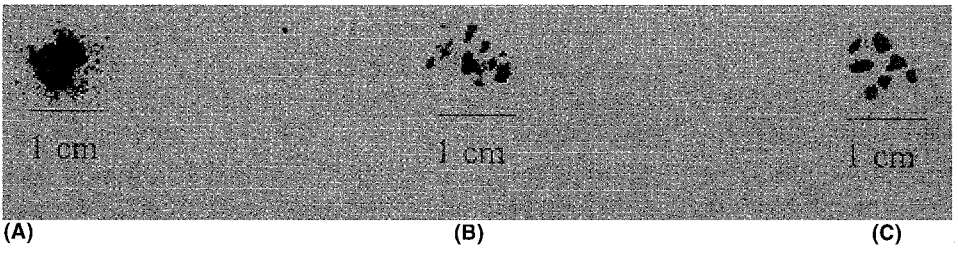

FIG. 15. Carbon nanofiber agglomerates after unloading from the reactor: (A) powdery material; (B) particles of low mechanical strength; (C) particles of high mechanical strength. (Reproduced from Ref. 22.)

The discrete carbon bodies shown in Fig. 15C display a bulk crushing strength of 1 MPa that makes them suitable for use as a support for fixed-bed applications.

The patent by Moy and Chishti [55] gives some other experimental clues between the catalyst characteristics and the agglomerates. Planar support particles give rise to "combed yarn" fiber aggregates, in line with work on macroscopic surfaces [56]. A support material of low mechanical strength, on the other hand, leads to entangled "bird nest" structures. Some of these phenomena remind one of the morphology developments of polymers when using heterogeneous catalysts.

The study by Kushinov et al. [54] reveals that within a single macroscopic body, a gradient in the extent of interweaving of fibers may occur. A more open structure of fibers is apparent closer to the outer surface of the growing granule. Another interesting finding of this research relates to the effect of growing time on mechanical properties. These workers note that initially a weak granule is formed, but prolonged growth enhances the mechanical strength. Furthermore, they note that a higher nickel-to-support ratio in the starting material leads to a higher attrition resistance of the produced granules.

Working with a fluid-bed reactor, Parmon and co-workers [57] use inert material to prevent extensive agglomeration of granules. Apparently, in a fluid-bed reactor thus operated, a more or less constant granule size that no longer directly correlates to the initial catalyst body size can be realized. Granule fracture appears to occur in this kind of system.

In general, one can say that the carbon granules will be highly porous, with mesopores and macropores being present between the nanofibers. Uniquely high porosities can be thus obtained while mechanical strength is still high. If a higher density of fibers is wanted (e.g., because of high surface area per unit of volume is needed), techniques from colloid chemistry can be used. Shaffer et al. [53] report that proper dispersion (sometimes leading to gellike structures) followed by filtration can lead to densification of the fibers related to aligning of the nanofibers. Also, simple drying can lead to a coherent solid that can be easily shaped in macroscopic bodies that can be handled.

Well-aligned carbon nanofibers can also be grown directly. Li et al. [58] used iron in mesoporous silica, whereas Ren et al. [56] applied a flat nickel-coated glass surface and Li et al. [59] used cobalt in the pores of an anodic aluminum oxide template.

IV. APPLICATIONS

A. *Survey of Applications*

The work on applications of carbon nanofibers or nanotubes has been stimulated enormously by the article by Iijima [4]. In his work, arc-discharge techniques have been used to produce nanotubes. Recently, workers have realized that the catalytic methods described in this review are much more promising for producing nanofibers or nanotubes in large quantities at realistic costs.

The number of applications of catalytically grown carbon nanofibers can be divided into four large areas (viz. in electronic components, as polymer additive, for gas storage, and as catalyst support material). In this section, we briefly survey the first three areas; we expand on the latter in the next section.

The number of potential applications in electronic devices is large and will not be reviewed here. As a typical example, we mention the study of high-power electrochemical capacitors by Niu et al. [60]. Related to this, one studies applications in lithium-ion batteries and in fuel-cell electrodes [61]. Tennent [31] mentions the preparation of high-surface-area electrodes and shielding of objects from electromagnetic radiation.

Carbon nanofibers display unique mechanical and electrical properties that have triggered the search for applications in composite materials. Enforcement of materials as well as enhancement of electrical conductivity is actively considered [31]. In order to enhance polymer conductivity, one can add well-known conventional carbon fibers with micrometer thickness. Using nanofibers enables one to achieve enhanced conductivity at a much reduced loading of carbon (Fig. 16).

Gas storage using carbon nanotubes or nanofibers has attracted a great deal of attention, invoking an article title as "The World's Smallest Gas Cylinders?" [62]. In a very elegant experiment, Gadd et al., using hot isostatical pressing of argon (923 K, 170 MPa), observed argon in the "closed" tubes that was retained after cooling and depressurizing.

For future applications, hydrogen storage may become very important in the

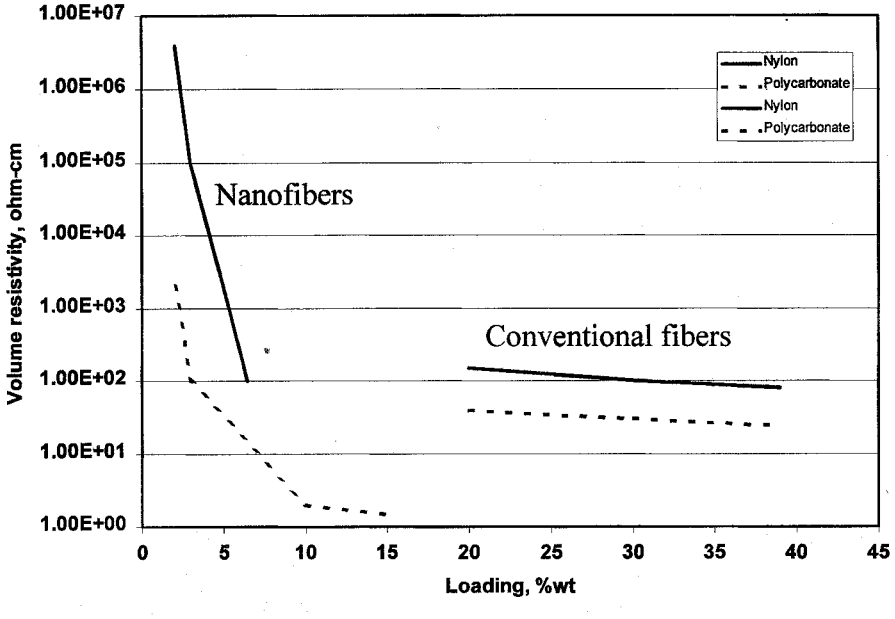

FIG. 16. Improvement of the electrical conductivity of plastics by the addition of carbon fibers; conventional fibers versus nanofibers. (Data from Hyperion Catalysis.)

context of renewable energy. A preliminary study by Dillon et al. [63] seemed to indicate that adsorption of molecular hydrogen at temperatures around ambient and pressures below atmospheric occurs in carbon single-walled nanotubes (SWTN) produced by the arc-discharge method. The low content of SWTN (0.1 wt%) and the high content of cobalt (~20 wt%) substantially complicated the establishment of an unambiguous relation between hydrogen storage and carbon structure, however.

Exciting results by Chambers et al. [64] suggest huge uptakes of hydrogen at ambient temperatures and a pressure of 12 MPa and below. The maximum uptake quoted amounted to ~20 NL(H_2)/g(carbon), which corresponds to a stoichiometry of H/C = 21 at/at. It is noteworthy that an earlier patent [65] provides examples of hydrogen uptake with carbon nanofibers of only 20 N mL/g, a factor of 1000 lower than in the quoted paper. In Ref. 64, the authors suggest that critical to the elevated hydrogen uptake is the spacing between graphite layers of herringbone fibers of 0.337 nm, a distance characteristic for turbostratic graphite. It is noted that the authors suggest penetration of hydrogen between the graphite layers. Unfortunately, work by other researchers has not been successful to sustain these hydrogen uptake claims, neither on an experimental nor on a theoretical basis. An exception to the latter rule is the most recent article by Fan and co-workers [66], who measured uptake capacities of 1.4–1.8 NL/g. These capacities are still very high albeit a factor of 10 lower than described by Chambers and co-workers. In our opinion, all of these results might have been plagued by experimental problems often encountered when working with hydrogen at high pressures.

Yet another puzzling article on hydrogen storage has been published recently. Chen and co-workers [67] claim hydrogen uptakes of ~3 NL(H_2)/g(carbon) on Li-doped carbon nanotubes (H/C = 3 at/at) produced from methane over Ni/MgO. The hydrogen was adsorbed at around 773 K at ambient pressure. Dissociative adsorption of hydrogen was claimed to play a role in this system.

B. Carbon Nanofibers as Catalyst Support Materials

Carbon is an important support material in heterogeneous catalysis, in particular for liquid-phase catalysis. Activated carbon made from natural materials is used widely in this respect. The reproducibility as well as the microporosity of activated carbon has often hampered catalyst development. Carbon nanofibers can be produced on a large scale (Sect. V) in a reproducible manner with unique options to steer the metal–support interactions, lyophilicity, and texture.

During the last 5 years, we have seen the first studies in which carbon nanofibers (CNF) have been used as catalyst support materials. In 1994, Rodriguez and co-workers [51] published an article in which they used fibers grown from synthesis gas and iron as the catalyst at temperatures of 873 K. Introduction of an active phase (Fe or FeCu) onto the CNF was done via an incipient-wetness technique, followed by calcination and reduction. In comparison with alternative supports (γ-alumina and activated carbon), the FeCu/CNF catalyst displayed an

order of magnitude higher activity for ethene hydrogenation. The authors ascribed this activity enhancement to a unique metal–support interaction between the FeCu particles and the basal-plane regions of the CNF. Unfortunately, the authors do not provide characterization data that exclude alternative explanations for the activity differences, such as a limited extent of reduction for the FeCu/γ-Al_2O_3 catalysts.

In the same year, Planeix and co-workers [68] prepared Ru/C catalysts based on carbon nanotubes. The latter material had been obtained on the cathode in an arc-discharge experiment. The average Ru-particle size as deduced from TEM and H/Ru measurements was 3.5 nm. In the hydrogenation of cinnamaldehyde, a selectivity to cinnamyl alcohol of 92 was maintained at conversion levels up to 80%. This selectivity is much higher than that observed with conventional Ru/C catalysts. A metal–support interaction between Ru and C was suggested as a possible explanation for these very interesting observations.

More recent work of Park and Baker [69] focuses on the use of platelet-type fibers exposing exclusively graphite edge sites. Using a phosphorus-based treatment, preferential blocking of so-called armchair faces occurs. Deposition of nickel onto the thus modified CNF enabled one to conclude that the nickel particles active for hydrogenation of light alkenes reside on the zigzag faces. More characterization work is needed to substantiate these interesting claims.

Hoogenraad and co-workers [22,49,50,70] have carried out, by far, the most extensive work on CNF as carbon support material. A driving force for exploring CNF supports was related to the replacement of active carbon as support for liquid-phase catalysis. Activated carbon is a support with chemical properties difficult to control and, sometimes, cumbersome mechanical properties. The latter may lead to filtration problems in slurry-based processes. Hereafter, we will describe in detail the results obtained in these studies that focus on Pd/CNF catalysts for liquid-phase hydrogenation reactions [22].

Carbon fibers have been grown from synthesis gas ($H_2/CO = 0.33$ v/v) over iron-based catalysts at 843 K, leading to fibers of the parallel type. As discussed earlier, the parallel fibers display a high mechanical strength. A uniform fiber diameter of about 12 nm is obtained related to the uniform particle size of the iron catalyst used. The surface area of the fibers amounts to 225 m^2/g and the mesopore volume to 1.6 mL/g, from which an average pore diameter of 28 nm follows (cylindrical pore model).

The agglomerate particle size of the CNF samples in this study amounted to an average of 8 μm. From TEM, it followed that the fibers had formed open, tangled skeins that lead to strong bodies. A direct measure of the attrition resistance was obtained by comparing the particle size distribution (PSD) before and after ultrasonic treatment in ethanol. For the CNF support, no shift of the PSD is apparent, whereas with an activated carbon (AC) support, severe attrition is apparent. In Fig. 17, we compare the PSD after ultrasonic treatment of the CNF and of the AC support. Clearly, AC displays a much broader PSD with, moreover, a significant number of fines (<5 μm). Another measure of the mechanical integ-

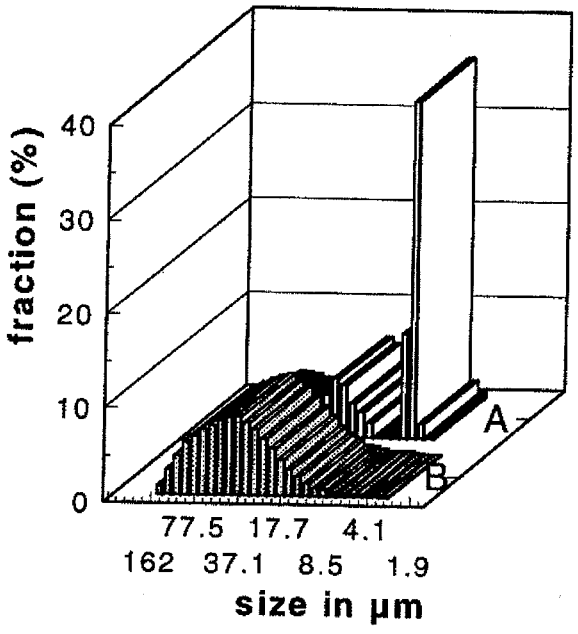

FIG. 17. Particle size distribution as determined by light scattering of carbon nanofibers (A) and active carbon (B) after ultrasonic treatment of the materials for 90 min in ethanol. (Reproduced from Ref. 22.)

rity of the catalysts comes from filtration measurements (Fig. 18). Clearly, the CNF support is better filterable than is the AC support.

As-synthesized CNF materials are hydrophobic and, as such, it is difficult to emplace an active phase. Therefore, an oxidative treatment under reflux in boiling nitric acid was applied to introduce polarity in the surface. The extent of oxygen introduction was assessed from thermogravimetric analysis of the fibers in an inert atmosphere. Over a wide temperature range (373–1273 K), a weight loss by the formation of CO and CO_2 is apparent. The weight loss is plotted against the reflux time in Fig. 19, showing a linear increase with time. From other characterization techniques, it has turned out that at least part of the oxygen is present as carboxylic acid groups.

Palladium has been introduced by ion exchange with a Pd–ammonia complex at pH = 5–6. A metal load of 2.5–3 wt% was thus obtained. It appeared crucial to carry out all synthesis steps under nitrogen. Especially during drying under air, extensive sintering of Pd took place. TEM and extended x-ray absorption fine structure (EXAFS) studies [22,70] have shown that hydrogen-reduced Pd/CNF prepared carefully contains 1.5-nm particles with significant interaction between Pd and the support (hemispherical metal particles).

Hoogenraad [22] has carried out catalytic measurements for the hydrogenation of nitrobenzene to aniline. For an understanding of the catalysis measure-

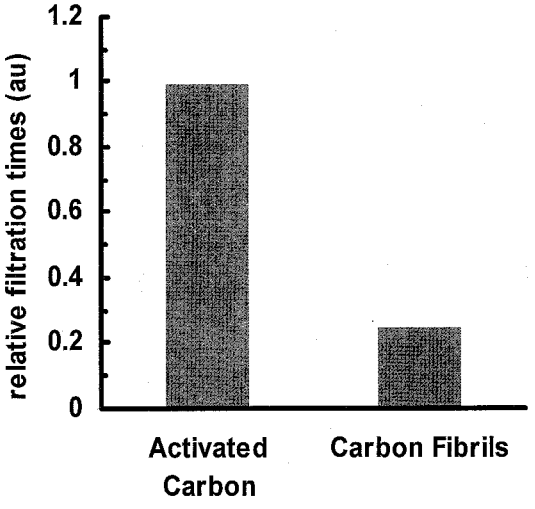

FIG. 18. Relative filtration rates of active carbon and carbon nanofibers. (Data from Ref. 22.)

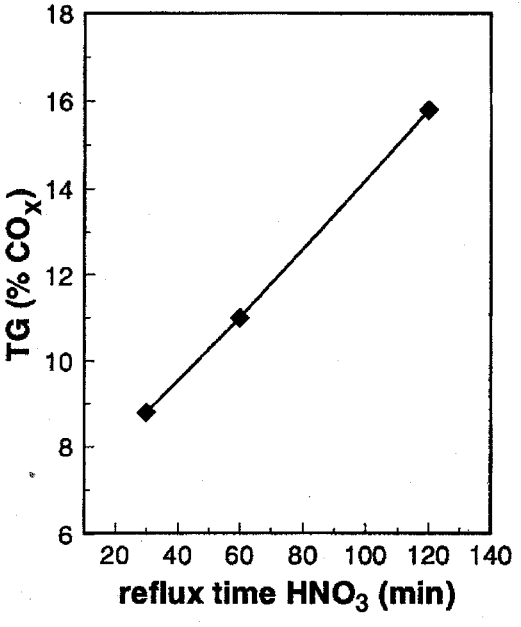

FIG. 19. Weight loss of carbon nanofibers due to formation of CO/CO_2 during heating in argon from ambient conditions to 1353 K as a function of the reflux time in 65% nitric acid. (From Ref. 22.)

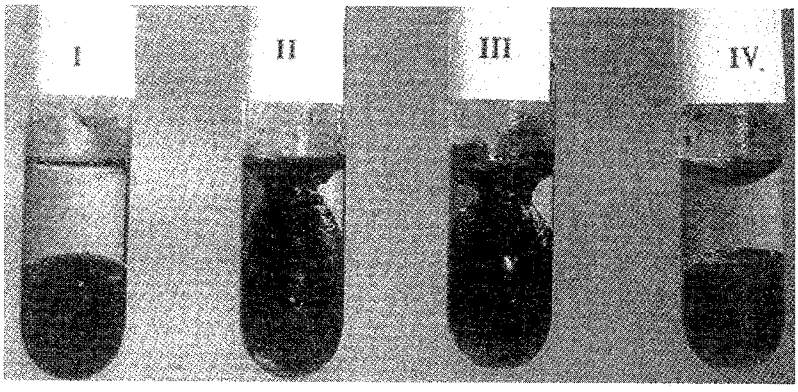

FIG. 20. Parallel carbon nanofibers dispersed in biphasic water (top) and nitrobenzene (bottom) system: I: fibers as-grown; II: fibers refluxed in nitric acid; III: fibers refluxed in nitric acid and kept in argon at 523 K; IV: refluxed in nitric acid and kept in argon at 673 K. (Reproduced from Ref. 22.)

ments, it is necessary that we first focus on the lyophilicity of the CNF supports. In Fig. 20, we show results for differently pretreated CNF supports in contact with a biphasic water (top) and nitrobenzene (bottom) system. The freshly grown CNF concentrate in the organic phase, thus revealing its hydrophobic nature. After nitric acid oxidation, the fibers are distributed over both phases with preference for the interfaces present. The right-hand-side tube shows that oxidized fibers subsequently heated in an inert atmosphere at 673 K are again hydrophobic due to loss of surface oxygen.

Catalysis of hydrogenation of pure nitrobenzene at room temperature using Pd/CNF reduced at 523 K and 673 K, respectively, revealed a threefold activity enhancement due to the higher reduction temperature. The explanation put forward by the authors relates to the interaction between liquid and support: The lower polarity of the high-temperature reduced sample leads to a higher lyophilicity in nitrobenzene.

In a more extensive study, Hoogenraad [22] compared the hydrogenation activity of Pd/CNF (fishbone), Pd/CNF (parallel), and Pd/AC. (See Fig. 21). Surprisingly, the fishbone-type fibers display, even with a lower Pd content, a much higher activity than Pd/AC and the parallel fibers. Unfortunately, as in the work of Rodriguez [51], insufficient characterization data are available to explain these interesting phenomena in detail.

Leaving now the extensive work of Hoogenraad, we finally refer to the most recent work of Teunissen and Geus to "equip" carbon fibers with a magnetic nucleus to enable separation from the liquid or gas phase using a magnetic field [71]. By using soft magnetic alloys, in particular NiFe, they prevent clustering of particles due to remnant magnetism. These magnetic carbon fibers (or carbon particles) have been used to produce, again, Pd/C catalysts with interesting catalytic properties.

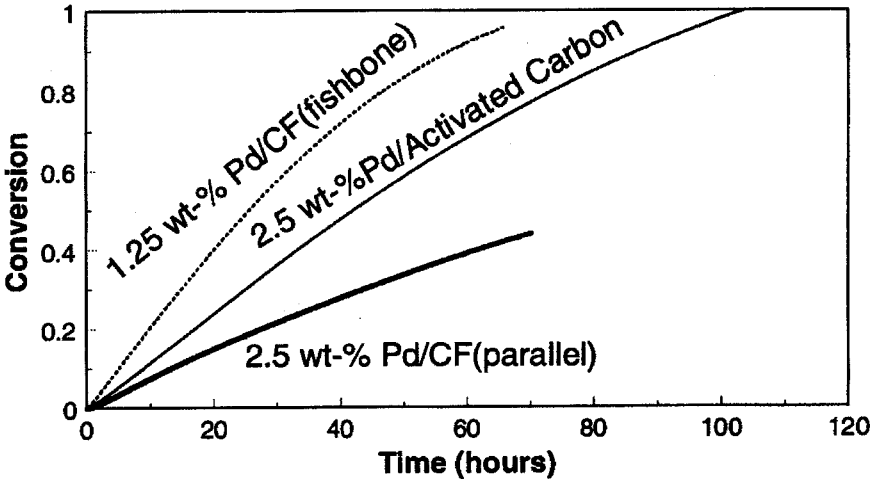

FIG. 21. The conversion of nitrobenzene to aniline at 298 K as a function of time using different Pd/C catalysts. (Reproduced from Ref. 22.)

Although progress has been made using carbon nanofibers as catalyst support materials, much work has to be done to fully exploit these materials. Moreover, production costs of the fibers should be reasonable. We discuss this in the next section.

V. LARGE-SCALE PRODUCTION OF CARBON NANOFIBERS

In this section, we deal with the issues regarding the large-scale production, including the production costs of carbon nanofibers. Specific issues that determine the technology and economics are the types of fiber grown, the reactor type, the nature of the carbon-containing gas, the reaction time and temperature, and the yield of carbon fibers. We will first discuss the most important articles—in particular, patents and patent applications that provide the building blocks of the technology and economy of large-scale production.

Geus [39] has been granted a patent related to the growth of fishbone-type fibers using mainly nickel-based catalysts. These materials may be advantageously used as catalyst support material, as the edge planes can be functionalized to anchor supported metals.

Tennent [31], working for Hyperion Catalysis International (HCI), has claimed parallel fibers grown at temperatures between 1123 and 1473 K yields carbon over catalytic iron (alloy) metal larger that 100 m/m. In the examples of this patent, the author has used a typical laboratory setup for fiber growth (viz.

a horizontal tube with a ceramic boat to hold the catalyst powder). It is not clear why the authors apply such high temperatures in the examples. The reason that the parallel-type fibers are claimed is related to their high mechanical strength that makes them useful in the reinforcement of matrices. This is in line with the commercial use of the HCI fibers as polymer additives.

Synder et al. [32], again for HCI, have applied for a patent that is complementary to the one by Tennent [31]. The parallel-fibers Fe-based catalysts are now grown at more modest temperatures of 673–1123 K, preferably of 873–1023 K. The reactor used in the examples is a vertical fixed-bed type with gas downflow and glass wool above the porous support grid. The glass wool probably serves to prevent blocking of the support grid by growing nanofibers.

The third patent applied for by HCI is by Moy and Chishti [55]. The issue dealt with here is to enhance the carbon yield by modification of the growth catalyst. In particular, the addition of (Mg, Al) carboxylates boosts the yield to the range 15–25 m/m basis catalyst or 75–250 m/m basis iron metal. Again a fixed-bed reactor is used in the examples. An interesting detail mentioned is the use of carbon nanofibers as support material for the catalytic metal. In this way, one prevents contamination of the fibers produced with refractory, oxidic support material.

Having summarized the most important patent literature, we briefly mention some facts from the open literature related to the reactors used for growth of carbon nanofibers. Baker et al. [29] have used a horizontal setup similar to the one described by Tennent [31]. Hoogenraad [22] had applied a fixed-bed setup, but he mentioned that a cylindrical reactor suffers from breakage due to the expansion of the (strong) fibers. For that reason, he used a spherical glass vessel with a porous support plate. In general, we note that the use of a fixed-bed reactor will lead inevitably to a batch-type operation. The use of a moving-bed reactor may alleviate this problem, but, in general, this puts a strong demand on the catalyst characteristics—in particular, mechanical strength and the spherical shape of the catalyst and the fiber agglomerates.

Workers from the Boreskov Institute in Russia have done interesting work growing fibers using a fluid-bed reactor [57]. They have developed the catalytic decomposition of natural gas at moderate temperatures (723–923 K) using Ni-based catalysts. Granulated carbon is produced with sizes of 1–5 mm. In order to prevent agglomeration of the growing particles, some "inert substrates" have been added. An integrated pilot plant (reactor volume 5 L) recycling unreacted natural gas has been operated. A wide range of carbon fiber yield has been claimed: 50–400 m/m basis catalyst intake. An especially attractive feature of this type of reactor is that continuous operation is within reach. The addition of a growth catalyst and withdrawal of carbon fiber product can be envisaged.

Turning now to the large-scale production and related costs of carbon nanofibers, we speculate that the only commercial producer of carbon nanofibers today (HCI) uses (modified) fixed-bed technology. We feel that substantial cost savings can be envisaged by making use of continuous fluid-bed operation.

TABLE 2
Results of Production-Cost Estimates for Carbon Nanofibers As-Grown for a High- and a Low-Cost Scenario

Case	High cost	Low cost
Scale of production	Low	High
Reactor type	Fixed bed	Fluidized bed
Type of operation	Batch	Continuous
Yield of fibers (m/m)	50	200
Growth time (h)	2	0.5
Cost estimate (US$/kg)	>50	<10

The economics will be dictated by a large number of factors. The most important ones are the following:

- The scale of production
- The feedstock used (e.g., ethene or natural gas)
- The reactor type and related type of operation
- The yield of carbon nanofibers scaled to the intake of catalytic metal
- The reaction time and temperature

By using high- and low-cost scenarios, based on an extensive study of the literature, we have made back-of-the-envelope cost estimates, the results of which are shown in Table 2. Price quotes by HCI are in line with the case of high costs [viz. 50 US$/kg (fibers blended in polymer)]. The high-cost case rules out the use of carbon nanofibers for large-volume applications, such as material enforcement, catalyst support material, and gas storage. The use of the technology/process indicated as low-cost scenario (<10 US$/kg) indicates, however, that these large-volume applications are within reach. Even the competition with active carbon for noble-metal supported catalysts can be envisaged as a particular case in point.

VI. OUTLOOK AND FUTURE RESEARCH

The review presented gives a number of clues for future potential of and research on carbon nanofibers. Here, we will focus on some items that also hold industrial perspectives.

Up until now, wide application of carbon nanofibers has been inhibited by high production costs. Large-scale, low-cost production calls for continuous operation of using, for example, fluid-bed technology at a significant scale. In view of the expanding catalyst particles, the design of such a fluid-bed reactor is not at all trivial. Engineering research will be needed, along with catalysts and materials research.

Each particular application calls for extensive R&D. The use of CNF as catalyst support material holds great potential [72,73]. However, detailed knowl-

edge of the surface structure of the CNF is needed. For example, what are the terminating groups with fishbone-type fibers? How can we easily functionalize these edges and thereby anchor metals or metal complexes. Metal–support interactions are now accessible for the study of carbon at a new level of detail.

The tertiary structure of carbon nanofibers agglomerates is important for many applications. Although the fibers are mechanically strong on an individual basis, the strength of agglomerates depends on factors such as the extent of interweaving. More knowledge is needed on how to control this. Large, strong particles would open up the use of CNF as support material for fixed-bed catalysts.

Last but not least, fundamental research on the formation and structure of carbon nanofibers will be continued. *In situ* spectroscopy is advocated for revealing further details on the carbon–metal interaction during fiber nucleation and growth. The structural details and morphology of the carbon fibers will be studied by three-dimensional transmission electron microscopy (3D-TEM) currently under development for the study of complex materials [74].

VII. CONCLUSIONS

From this review, it is apparent that graphitic carbon nanofibers can be grown with widely varying properties using metallic catalysts and carbon-containing gases. The mechanism of growth always involves dissociation of the gas at the metal surfaces, followed by dissolution of carbon into the bulk, followed by diffusion to the surface of the particle where graphite is precipitated. Both the thermodynamics of the steady-state growth as well as the nucleation phase are now reasonably well understood.

Two fundamentally different types of fibers can be grown (viz. parallel and fishbone type). The thickness of the fibers relates to the metal particle size, and the orientation of the graphite plane can be steered by the growth temperature and/or the nature of the metal. Iron tends to give parallel fibers, whereas nickel often leads to fishbone-type fibers.

The structure of carbon nanofibers agglomerates strongly affects the mechanical strength at a macroscopic scale. Fast growth of thin fibers leads to weak particles; slow growth of thick fibers leads to strong particles.

Applications of carbon nanofibers envisaged today are manifold and can be divided broad brush into materials additives, gas storage, electronic devices, and catalyst support materials. To the best of our knowledge, the first commercial application is as a polymer additive, but many more are within reach, in line with current intense research efforts.

The commercial production of carbon nanofibers on a limited scale can be carried out in a fixed-bed reactor, leading to production costs around 50 US$/kg. Large-scale production using fluid-bed technology could well lead to a fivefold or more cost reduction (i.e., costs of 10 US$/kg or less). This would open up large-volume applications such as in gas storage and as catalyst support material.

ACKNOWLEDGMENTS

We are grateful for the discussions with Dr. A. J. van Dillen, Dr. W. Teunissen, Dr. M. G. Nijkamp, and Dr. T. G. Ross. We gratefully acknowledge support by Shell International Oil Products. This work has been carried out under the auspices of the Netherlands Research Institute on Catalysis (NIOK), report NIOK-99-03-04.

REFERENCES

1. T. V. Hughes and C. R. Chambers, U.S. Patent 405,480 (1889).
2. S. D. Robertson, *Nature, 221*, 1044 (1969).
3. J. R. Rostrup-Nielsen, *J. Catal., 85*, 31 (1984).
4. S. Iijima, *Nature, 354*, 56 (1991).
5. T. W. Ebbesen (ed.), *Carbon Nanotubes. Preparation and Properties*, CRC Press, New York, 1997.
6. P. M. Ajayan, *Chem. Rev., 99*, 1787 (1999).
7. D. L. Trimm, *Catal. Rev.—Sci. Eng., 16*, 155 (1977).
8. J. R. Rostrup-Nielsen and D. L. Trimm, *J. Catal., 48*, 155 (1977).
9. C. H. Bartholomew, *Catal. Rev.—Sci. Eng., 24*, 67 (1982).
10. J. L. Figueiredo, *Erdöl Kohle–Erdgas–Petrochem. 42*, 294 (1989).
11. R. T. K. Baker, in *Carbon Fibers, Filaments and Composites* (J. L. Figueiredo, C. A. Bernardo, R. T. K. Baker, and K. J. Hüttinger, eds.), NATO ASI Series, Kluwer, Dordrecht, 1990, p. 405.
12. N. M. Rodriguez, *J. Mater. Res., 8*, 3233 (1993).
13. R. T. K. Baker, P. S. Harris, R. B. Thomas, and R. J. Waite, *J. Catal., 30*, 86 (1973).
14. A. Sacco, P. Thacker, T. N. Chang, and A. T. S. Chiang, *J. Catal., 85*, 224 (1984).
15. P. K. de Bokx, A. J. H. M. Kock, E. Boellaard, W. Klop, and J. W. Geus, *J. Catal., 96*, 454 (1985).
16. A. J. H. M. Kock, P. K. de Bokx, E. Boellaard, W. Klop, and J. W. Geus, *J. Catal., 96*, 468 (1985).
17. I. Alstrup and J. R. Rostrup-Nielsen, *J. Catal., 100*, 545 (1986).
18. I. Alstrup, *J. Catal., 109*, 241 (1988).
19. F. J. Dent, L. A. Moignard, A. H. Eastwood, and W. H. Blackburn, *Trans. Inst. Gas Eng.*, 602 (1945–1946).
20. J. R. Rostrup-Nielsen, *J. Catal., 27*, 343 (1972).
21. J.-W. Snoeck, G. F. Froment, and M. Fowles, *J. Catal., 169*, 240 (1997).
22. M. S. Hoogenraad, Ph.D. thesis, Utrecht University (1995).
23. S. H. Lee and E. Ruckenstein, *J. Catal. 107*, 23 (1987).
24. M. Audier, A. Oberlin, and M. Coulon, *J. Crystal Growth, 55*, 549 (1981).
25. F. C. Schouten, E. W. Kaleveld, and G. A. Bootsma, *Surf. Sci., 63*, 460 (1977).
26. F. C. Schouten, O. L. J. Gijzeman, and G. A. Bootsma, *Surf. Sci., 87*, 460 (1979).
27. V. I. Zaikovskii, V. V. Chesnokov, and R. A. Buyanov, *Appl. Catal., 38*, 41 (1988).
28. R. T. Yang and J. P. Chen, *J. Catal., 115*, 52 (1989).
29. R. T. K. Baker, M. S. Kim, A. Chambers, C. Park, and N. M. Rodriguez, *Studies Surf. Sci. Catal., 111*, 99 (1997).

30. N. M. Rodriguez, A. Chambers, and R. T. K. Baker, *Langmuir, 11*, 3862 (1995).
31. H. G. Tennent, U.S. Patent 4,663,230 (1987).
32. C. E. Snyder, W. H. Mandeville, H. G. Tennent, L. K. Truesdale, and J. J. Barber, WO Patent Appl. 89/07163 (1989).
33. J.-F. Colomer, P. Piedigrosso, I. Willems, C. Cournet, P. Bernier. G. Van Tendeloo, A. Fonseca, and J. B. Nagy, *J. Chem. Soc., Faraday Trans., 94*, 3753 (1998).
34. A. Fonseca, K. Hernadi, J. B. Nagy, D. Bernaerts, and A. A. Lucas, *J. Molec. Catal. A, 107*, 159 (1996).
35. K. Hernadi, A. Fonseca, J. B. Nagy, D. Bernaerts, A. Fudula, and A. A. Lucas, *Zeolites, 17*, 416 (1996).
36. A. Thaib, G. A. Martin, P. Pinheiro, M. C. Schouler, and P. Gadelle, *Catal. Lett., 63*, 135 (1999).
37. Y. H. Hu and E. Ruckenstein, *J. Catal., 184*, 298 (1999).
38. P. Chen, H.-B. Zhang, G.-D. Lin, Q. Hong, and K. R. Tsai, *Carbon, 35*, 1495 (1997).
39. J. W. Geus, Eur. Patent 0,198,558,B1 (1985).
40. E. Boellaard, P. K. de Bokx, A. J. H. M. Kock, and J. W. Geus, *J. Catal., 96*, 481 (1985).
41. E. Tracz, R. Scholz, and T. Borowiecki, *Appl. Catal., 66*, 133 (1990).
42. J.-F. Colomer, G. Bister, I. Willems, Z. Konya, A. Fonseca, G. Van Tendeloo, and J. B. Nagy, *Chem. Commun.*, 1343 (1999).
43. B. Kitiyanan, W. E. Alvarez, J. H. Harwell, and D. E. Resasco, *Chem. Phys. Lett., 317*, 497 (2000).
44. T. Abatemarco. J. Stickel, J. Belfort, B. P. Frank, P. M. Ajayan, and G. Belfort, *J. Phys. Chem. B, 103*, 3534 (1999).
45. Z. Jia, Z. Wang, J. Liang, B. Wei, and D. Wu, *Carbon, 37*, 903 (1999).
46. S. Amelinckx, X. B. Zhang, D. Bernaerts, X. F. Zhang, V. Ivanov, and J. B. Nagy, *Science, 265*, 635 (1994).
47. X. Chen and S. Motojima, *Carbon, 37*, 1817 (1999).
48. S. Motojima and Q. Chen, *J. Appl. Phys., 85*, 3919 (1999).
49. M. S. Hoogenraad, M. F. Onwezen, A. J. van Dillen, and J. W. Geus, *Studies Surf. Sci. Catal., 101*, 1331 (1996).
50. M. S. Hoogenraad, R. A. G. M. M. van Leeuwarden, G. J. B. van Breda Vriesman, A. Broersma, A. J. van Dillen, and J. W. Geus, *Studies Surf. Sci. Catal., 91*, 263 (1995).
51. N. M. Rodriguez, M.-S. Kim, and R. T. K. Baker, *J. Phys. Chem., 98*, 13,108 (1994).
52. S. Inoue, N. Ichikuni, T. Suzuki, T. Uematsu, and K. Kaneko, *J. Phys. Chem. B, 102*, 4689 (1998).
53. M. S. P. Shaffer, X. Fan, and A. H. Windle, *Carbon, 36*, 1603 (1998).
54. G. G. Kuvshinov, Yu. I. Mogilnykh, D. G. Kuvshinov, D. Yu. Yermakov, M. A. Yermakova, A. N. Salanov, and N. A. Rudina, *Carbon, 37*, 1239 (1999).
55. D. Moy and A. Chishti, WO Patent Appl. 93/24687 (1993).
56. Z. F. Ren, Z. P. Huang, J. W. Xu, J. H. Wang, P. Bush, M. P. Siegal, and P. N. Provencio, *Science, 282*, 1105 (1998).
57. V. N. Parmon, G. G. Kuvshinov, V. A. Sadykov, and V. A. Sobyanin, *Studies Surf. Sci. Catal. 119*, 677 (1998).
58. W. Z. Li, S. S. Xie, L. X. Qian, B. H. Chang, B. S. Zhou, W. Y. Zhuo, R. A. Zhao, and G. Wang, *Science, 274*, 1701 (1996).
59. J. Li, M. Moskovits, and T. L. Haslett, *Chem. Mater., 10*, 1963 (1998).

60. C. Niu. E. K. Sichel, R. Hoch, D. Moy, and H. Tennent, *Appl. Phys. Lett., 70*, 1480 (1997).
61. G. Che, B. B. Lakshmi, E. R. Fisher, and C. R. Martin, *Nature, 393*, 346 (1998).
62. G. E. Gadd, M. Blackford, S. Moricca, N. Webb, P. J. Evans, A. M. Smith, G. Jacobson, S. Leung, A. Day, and Q. Hua, *Science, 277*, 933 (1997).
63. A. C. Dillon, K. M. Jones, T. A. Bekkedahl, C. H. Klang, D. S. Bethune, and M. J. Heben, *Nature, 386*, 377 (1997).
64. A. Chambers, C. Park, R. T. K. Baker, and N. M. Rodriguez, *J. Phys. Chem. B, 102*, 4253 (1998).
65. N. M. Rodriguez and R. T. K. Baker, US Patent 5,653,951 (1997).
66. Y.-Y. Fan, B. Liao, M. Liu, Y.-L. Wei, M.-Q. Lu, and H.-M. Cheng, *Carbon, 37*, 1649 (1999).
67. P. Chen, X. Wu, J. Lin, and K. L. Tan, *Science, 285*, 91 (1999).
68. J. M. Planeix, N. Coustel, B. Coq, V. Brotons, P. S. Kumbhar, R. Dutartre, P. Geneste, P. Bernier, and P. M. Ajayan, *J. Am. Chem. Soc., 116*, 7935 (1994).
69. C. Park and R. T. K. Baker, *J. Phys. Chem. B, 103*, 2453 (1999).
70. B. L. Mojet, M. S. Hoogenraad, A. J. van Dillen, J. W. Geus, and D. C. Koningsberger, *J. Chem. Soc., Faraday Trans., 93*, 4371 (1997).
71. W. Teunissen, A. A. Bol, and J. W. Geus, *Catal. Today, 48*, 329 (1999).
72. K. P. de Jong, *CatTech, 2*, 87 (1998).
73. K. P. de Jong, *Curr. Opin. Solid State Mater. Sci., 4*,55 (1999).
74. A. J. Koster, U. Ziesse, A. J. Verkleij, A. H. Janssen, J. de Graaf, J. W. Geus, and K. P. de Jong, *Stud. Surf. Sci. Catal, 130*, 329 (2000).